

Effect of Localised Wall Suction on the Small-scale Motion in a Turbulent Boundary Layer

O. Oyewola, L. Djenidi, P. Burattini and R.A. Antonia

Discipline of Mechanical Engineering
 University of Newcastle, NSW, 2308 AUSTRALIA

Abstract

Hot wire measurements have been made in a turbulent boundary layer subjected to concentrated suction applied through a porous wall strip in order to examine the influence of suction on the small-scale motion. The suction results show significant departure from the no-suction case of the Kolmogorov normalised spectra and second-order structure functions for $k^*_{1} < 0.2$ and $r^* > 20$, respectively, suggesting that suction induces a change in the small-scale motion. This change is a result of the weakening of the large-scale structures. The effect is enhanced as the suction rate is increased.

Introduction

The response of the large-scale motion to suction applied through a single narrow porous wall strip or slit has received some attention in the past [3,9,10,13]. For example, [3] studied the effect of concentrated wall suction, applied through a short porous wall strip, on a low Reynolds number turbulent boundary layer. They showed that, when the suction rate is sufficiently high, pseudo-relaminarisation occurs almost immediately downstream of the suction strip. Further downstream, transition occurs and is followed by a slow return to a fully turbulent state. Further, [9,10] showed that both the suction rate, σ ($\equiv V_w b / \theta_0 U_1$, where V_w is the suction velocity, b is the effective width of the strip, θ_0 is the momentum thickness of the boundary layer at the leading edge of the porous strip with no-suction and U_1 is the free stream velocity), and the momentum thickness Reynolds number, R_{θ_0} , played an important role in the relaminarisation process. They argued that the ratio R_{θ_0} / σ should not exceed a (as yet undetermined) critical value, if relaminarisation is to occur. Recently, the effect concentrated wall suction can have on the anisotropy of the Reynolds stress tensor was examined in [11]. Those results indicated that the large-scale motion of the boundary layer was significantly altered by suction, and that the global anisotropy of the layer increases with the suction rate. For example, they found that the shape of the structures near the wall changed from a cigar to a pancake-shape when suction is applied.

The characteristics of the small-scale motion in a smooth wall turbulent layer have been examined by several authors [1,2,17]. The possibility of local isotropy at various R_{θ_0} ($\equiv U_1 \theta_0 / \nu$, where, θ_0 and ν are the momentum thickness and kinematic viscosity of the fluid respectively) and the Taylor microscale Reynolds number R_{λ} ($\equiv ((u_1^2))^{1/2} \lambda / \nu$, where u_1 is the longitudinal velocity fluctuation, λ the longitudinal Taylor microscale, ν the viscosity of air) has spawned the introduction of various criteria for local isotropy [4,6,8,19]. For example, [19] used $S / ((\partial u / \partial y)^2)^{1/2}$ (where, $S \equiv \partial U / \partial y$) for characterising the anisotropy of the small-scale motion and suggested that this ratio should not depend on the Reynolds number in the near-wall region. Using direct numerical simulations of a fully developed channel flow, [1] showed that the magnitude of R_{λ} should have little effect on the degree of isotropy at sufficiently high wave number provided $S^* (\equiv S / ((\epsilon) / \nu)^{1/2}$, where $\langle \epsilon \rangle$ is the mean turbulent energy dissipation rate) is sufficiently small. They argued that the

Corrsin criterion is too restrictive and may be relaxed to $S^* \leq 0.2$, provided the high wave number vorticity spectra approach isotropy. However, the general consensus is that local isotropy is best satisfied at high R_{θ_0} and R_{λ} . Since changes in the boundary conditions affect R_{θ_0} , it would be of interest to determine if and how these changes influence the small-scale motion.

The main objective of the present study is to examine the influence of wall suction on the small-scale motion.

Measurement Details

Measurements were made in a smooth flat plate turbulent boundary layer, which is subjected to concentrated suction applied through a short porous strip. The turbulent boundary layer develops on the floor of the wind tunnel working section (figure 1) after it is tripped at the exit from a two-dimensional 9.5:1 contraction using a 100 mm roughness strip (Norton Bear No. 40, very coarse). Tests showed that the boundary layer was fully developed at the suction strip location, which is about 1200 mm downstream of the roughness strip. The roof of the working section is adjusted to achieve the desire pressure gradient (zero for the present investigation). The free stream velocity U_{∞} was approximately 7 ms^{-1} ; corresponding values of the initial momentum thickness Reynolds numbers R_{θ_0} are 1400 and the Taylor microscale Reynolds number is in the range $R_{\lambda} = 90-120$. A 3.25 mm thick porous strip with a width of 40 mm and made of sintered bronze with pore sizes in the range 40–80 μm or $(0.4-0.9)\nu / U_{\tau}$ was mounted flush with the test section floor. Allowing for the width of the mounting recess step, the effective width ($=b$) of the strip was 35 mm. Suction was applied through a plenum chamber located underneath the suction strip and connected to a suction blower, driven by a controllable DC motor, through a circular pipe (internal diameter $D = 130 \text{ mm}$ and $L/D \approx 38$, where, L , is the pipe length). The flow rate Q_r was estimated directly by radially traversing a Pitot tube located near the end of the pipe, for various values of the pipe centre-line velocity (U_c). A plot of Q_r vs U_c , allowed the suction velocity (V_w) to be inferred via the continuity equation ($Q_r = A_w V_w$, where, A_w is the cross-sectional area of the porous strip).

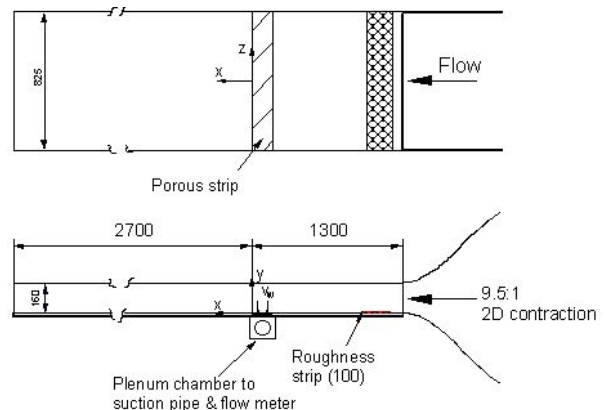


Figure 1: Schematic arrangement of the working section (dimensions in mm).

The suction velocity was assumed to be uniform over the porous surface; this assumption seems reasonable if the variation in the permeability coefficient of the porous material is $\pm 3\%$. Measurements were made for σ ($= V_w b / \theta_0 U_\infty$, normalised suction rate or severity index, as introduced by [3]) = 0, 0.8, 1.7, 3.3 and 5.5. The results for $\sigma = 0$ provided a reference against which the suction data could be appraised. The wall shear stress τ_w was measured with a Preston tube (0.72 mm outer diameter), and a static tube located approximately 35 mm above it at the same x position. The Preston tube was calibrated in a fully developed channel flow using a method similar to that described in [3,14]. τ_w was determined from the relation $\tau_w = -h(dp/dx)$, where h is the channel half-width and p is the static pressure. Although the calibration of the Preston tube in the channel flow may not ensure that τ_w will be correctly obtained especially if the flow is perturbed, the level of agreement with those inferred from the mean velocity gradient at the wall was about 5%. Measurements of the velocity fluctuations in the streamwise and wall normal directions were made with cross wires, each inclined at 45° to the flow direction. The etched portion of each wire (Wollaston, Pt-10% Rh) had a diameter of $2.5 \mu\text{m}$, and a length (l) to diameter ratio of about 200. The separation (Δ) between the inclined wires was about 0.6 mm. The ratios l/η and Δ/η for no-suction at $y^+ = 15$ are about 4.0 and 4.9 respectively. The velocity fluctuation in the spanwise direction was also measured by rotating the same X-probe through 90° . All hot wires were operated with in-house constant temperature anemometers at an overheat ratio of 1.5. The analog output signal of the hot wire was low pass filtered (the filter cut off frequency was typically between 5kHz and 8kHz), DC offset and amplified to within $\pm 5 \text{ V}$.

Mean Turbulent Energy Dissipation Rate and Mean Strain Rate

The variation of $\langle \epsilon \rangle \delta / U_\tau^3$ (δ is the boundary layer thickness) across the boundary layer is shown in figure 2 as a function of y/δ for both the perturbed and unperturbed boundary layers. The mean turbulent energy dissipation rate, $\langle \epsilon \rangle$, was estimated by integrating the dissipation spectrum (e.g., [18]), viz.

$$\langle \epsilon \rangle = 15\nu \int_0^\infty k_1^2 \phi_u(k_1) dk_1,$$

where $\phi_u(k_1)$ is the one-dimensional spectrum of the streamwise velocity. Taylor's hypothesis was used to obtain the one component wavenumber $k_1 = 2\pi f / U$, where U is the local mean velocity and f is the frequency. Because of the contamination due to electronic noise, the high wavenumber part of the spectrum was extrapolated by assuming an exponential decay function for the data corresponding to $k_1^{5/3} \phi_u$ [7,16]. It should be noted that a more reliable estimate of $\langle \epsilon \rangle$ would be to measure all the

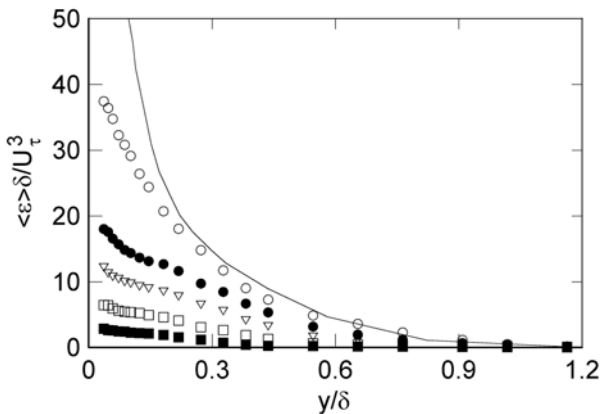


Figure 2: Variation of $\langle \epsilon \rangle \delta / U_\tau^3$ with σ . \circ , $\sigma = 0$; \bullet , 0.8; ∇ , 1.7; \square , 3.3; \blacksquare , 5.5; —: Spalart ($R_\theta = 1410$) [15].

components of $\langle \epsilon \rangle$ with multiple hot-wires. This is not feasible at the moment in the current laboratory experiment. The present data for $\sigma = 0$ fall below the DNS data of [15] at $R_\theta = 1410$ in the region $y / \delta \leq 0.2$ but there is reasonable agreement between the present measurement and the DNS data in the outer layer ($y / \delta > 0.4$). The reason for the discrepancy in the wall region is partly due to the inaccuracy of cross-wire measurements and the expected departure of $\langle \epsilon \rangle$ from its isotropic value. Because of the increased anisotropy of the near-wall flow, the uncertainty of $\langle \epsilon \rangle$ was estimated using error analysis to range between 45% and 19%, over the region $0.05 < y / \delta < 0.2$ for $\sigma = 0$. It is interesting to point out that the marginal difference between the present no-suction data of $\langle \epsilon \rangle$ and the DNS in the region $y / \delta > 0.2$ gives confidence in the values derived for the Kolmogorov's variables in that region. Thus, the comparison between the suction and no-suction data should be reliable, at least qualitatively, since the measurements were made with the same probe. The measurements should provide some insight into the changes that occur in the boundary layer. However, the comparison between the suction and no-suction data should be interpreted with caution.

Relative to no-suction, there is a considerable reduction in the normalised mean turbulent energy dissipation rate when suction is applied. This is consistent with the significant reduction observed in the production of the mean turbulent kinetic energy (not shown). These results suggest a possible alteration in the mechanism responsible for the energy transfer within the boundary layer, which in turn would affect both large and small-scale motions. This is not surprising since quasi-streamwise vortical structures are the major structural element responsible for turbulence production in the near-wall region. A reduction in $\langle \epsilon \rangle$ would imply a weakening of these structures. The effect is enhanced as σ is increased. The reduction in $\langle \epsilon \rangle$ is reflected in the Kolmogorov scales shown in figures 3a and 3b.

The figures are plotted in this manner to highlight the changes that occur in the near-wall region when suction is applied. Interestingly, the measured data agree reasonably well with the DNS data in the region $y^+ \geq 100$. η^+ varies only slowly nearly up to $y^+ \leq 100$ ($y / \delta \approx 0.2$).

While the rate of change of η^+ with y^+ , relative to $\sigma = 0$, increases as σ increases for $y^+ \geq 100$, that of ν_k^+ is reduced significantly. It seems that $y^+ = 100$ represents a transition point, above which the rate of change of η^+ or ν_k^+ is significantly increased for a particular σ . It may be concluded from the results presented here that, relative to no-suction, the near-wall structures of the perturbed boundary layer have been modified, as reflected in the changes in the energy dissipation rate and therefore the Kolmogorov velocity and length scales.

The variations with σ of R_λ and the Kolmogorov normalised shear S^* are shown in figure 4. All distributions of R_λ show

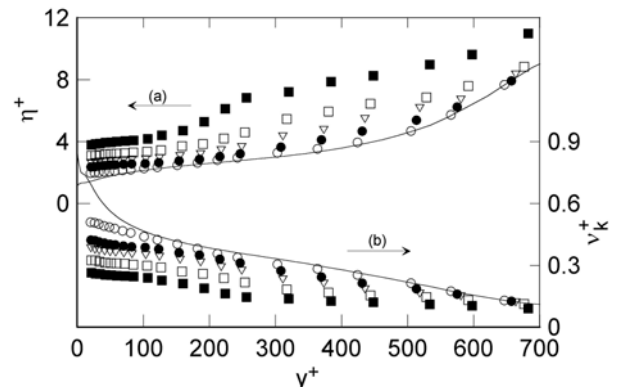


Figure 3: Variations of (a) η^+ ; (b) ν_k^+ with σ . Symbols are as in figure 2.

almost the same behaviour. R_λ decreases until a minimum is reached, increases again slightly and then decreases towards a constant value. The values are lower in the suction case as compared with no-suction case in the region $y / \delta \geq 0.05$. Similarly, relative to no-suction, S^* increases in the region $y / \delta < 0.45$ and decreases towards the negative values in the remaining part of the boundary layer when suction is applied.

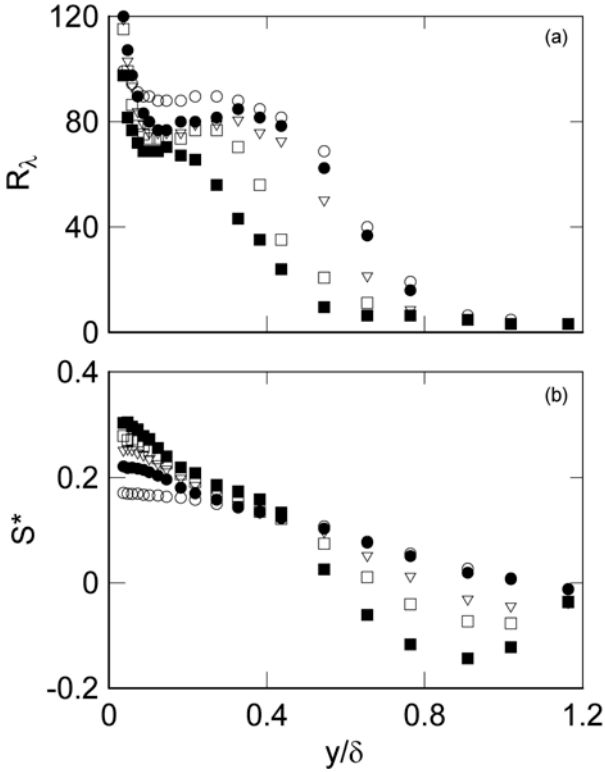


Figure 4: Variation of (a) R_λ ; (b) S^* with σ . Symbols are as in figure 2

The significant changes in R_λ and S^* when suction is applied would suggest that the small-scale motion has been altered, and the magnitude of this alteration is increased as σ is increased. For example, relative to no-suction, the change in the region $y / \delta \leq 0.2$, where R_λ and S^* , decreases and increases respectively when suction is applied may suggest an increase in the anisotropy of the small-scale. While S^* is about the same for all σ at $y / \delta \approx 0.43$, R_λ changes appreciably with σ . For example at $y / \delta \approx 0.43$, R_λ is 82, 78, 72, 35 and 24 for $\sigma = 0, 0.8, 1.7, 3.3$ and 5.5, respectively. The result could suggest that the anisotropy of the layer is the same at $y / \delta \approx 0.43$, and beyond this point, the anisotropy decreases below that for no-suction. This is evident in figure 4b where the suction data cross over below those of no-suction data at $y / \delta \approx 0.43$.

Spectra and Second-order Structure Functions

The distributions of $\langle \epsilon \rangle$, R_λ and S^* reflect a change in the near-wall structure when suction is applied. Figures 5 and 6 show the Kolmogorov compensated spectra and second-order structure functions, respectively, of u , v and w . Although, R_λ (90-120) is not large enough for the existence of a discernible inertial range, the dependence of $k_1^{*2} \phi_u^*$; $k_1^{*2} \phi_v^*$ and $k_1^{*2} \phi_w^*$ on σ is visible at low wavenumbers ($k_1^* < 0.2$), where the suction data depart from the no-suction data at $y / \delta = 0.125$ as shown in figure 5. The departure increases as σ increases. There is reasonable collapse among all the data sets at larger wavenumbers ($k_1^* \geq 0.2$) for the u spectra. The quality of the collapsed is poorer for v and w . This is not too surprising since the value of $\langle \epsilon \rangle$ used to calculate the

Kolmogorov scales were inferred from the u spectrum. However, the collapse should be addressed with some reservation because $\langle \epsilon \rangle$ obtained from $\langle \epsilon \rangle_{\text{hom}} \approx \nu \langle (\partial u / \partial x)^2 \rangle + \langle (\partial v / \partial x)^2 \rangle + \langle (\partial w / \partial x)^2 \rangle$ may provide a better estimate than those used here, and therefore, more appropriate. While the attenuations of the spectral at $k_1^* < 0.2$ by suction highlights a change in large-scale motion, the departure of v spectra further suggests the anisotropy of the large-scale resulting from an alteration of the large-scale structures. Since coherent structures are present at various scales, the departure from no-suction may suggest the weakening of these structures. Also, the attenuation of $k_1^{*2} \phi_v^*$ persists more than the other two over a significant fraction of k_1^* at least for $\sigma = 5.5$. Thus, the distributions of $k_1^{*2} \phi_v^*$ are more affected by suction than $k_1^{*2} \phi_u^*$ and $k_1^{*2} \phi_w^*$. The results are in agreement with [10]. The high-wavenumber variation exhibited among all the data set when displayed on a linear scale (not shown) may reflect the difference in large-scale anisotropy, since anisotropy introduced at the large scales can be felt down to the small scales. The effect of this change in the large-scale anisotropy increases as σ increases.

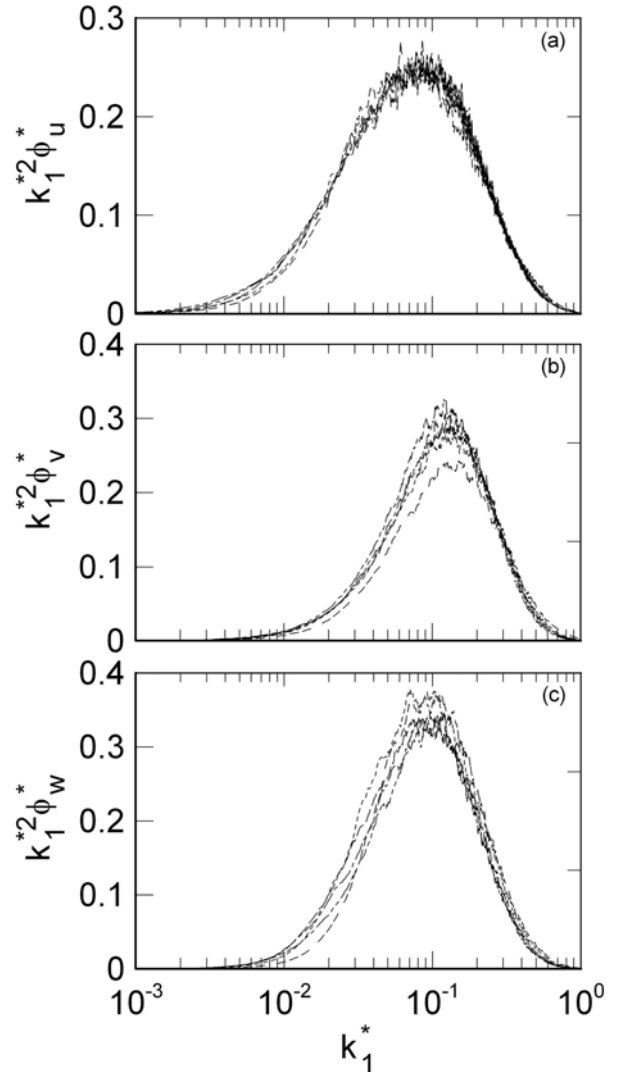


Figure 5: Kolmogorov-normalised spectra multiplied by k_1^{*2} , of (a) u , (b) v and (c) w for several values of σ at $y / \delta = 0.125$. —: $\sigma = 0$; — —: $\sigma = 0.8$; — — —: $\sigma = 1.7$; — — — —: $\sigma = 3.3$; — — — — —: $\sigma = 5.5$.

From figure 6, For $r^* \leq 10$, there is fairly good collapse among for $\langle (\delta u^*)^2 \rangle$, $\langle (\delta v^*)^2 \rangle$ and $\langle (\delta w^*)^2 \rangle$, providing support for the validation of Kolmogorov similarity hypothesis [18] in the

dissipative range even when the boundary layer is perturbed strongly.

In all the figures, there exist a region where there is no collapse among all the data set for $\langle(\delta u^*)^2\rangle$, $\langle(\delta v^*)^2\rangle$ and $\langle(\delta w^*)^2\rangle$ as σ increases, suggesting a change in the small-scale motion between the perturbed and unperturbed boundary layers. For example, in the range $r^* \geq 20$, the suction data depart from $\sigma = 0$ for $\langle(\delta u^*)^2\rangle$, $\langle(\delta v^*)^2\rangle$ and $\langle(\delta w^*)^2\rangle$, with $\langle(\delta v^*)^2\rangle$ and $\langle(\delta w^*)^2\rangle$ exhibiting the greater departures. Since v is a more sensitive indicator of the large-scale organization than u [12], the departures may suggest a difference in the anisotropy of the large-scale motion between suction and no-suction. For $\langle(\delta u^*)^2\rangle$, $\langle(\delta v^*)^2\rangle$ and $\langle(\delta w^*)^2\rangle$, the departure increases as σ is increased. It is likely that this large-scale anisotropic behaviour influences the isotropy of the smallest scales as observed in the poorer quality of collapse of the suction and no-suction data of $\langle(\delta v^*)^2\rangle$ in the region $r^* \leq 10$ (dissipative range) as compared with a reasonable collapse of $\langle(\delta u^*)^2\rangle$, suggesting that the change in the large-scale motion is felt down to the smallest scales. While the lack of collapse of $\langle(\delta v^*)^2\rangle$ may suggest differences in the anisotropy of the small-scale motion between suction and no-suction, the departures of $\langle(\delta w^*)^2\rangle$ from $\sigma = 0$ may not be attributed to a change in the anisotropy of the small-scale motion, but may rather highlight strictly the differences in the large-scale motion between the suction and no-suction. Also, taking into consideration that R_λ and the local mean shear are influenced by suction (see figure 4), the departures observed in $\langle(\delta u^*)^2\rangle$, $\langle(\delta v^*)^2\rangle$ and $\langle(\delta w^*)^2\rangle$ would also reflect the influence of these parameters.

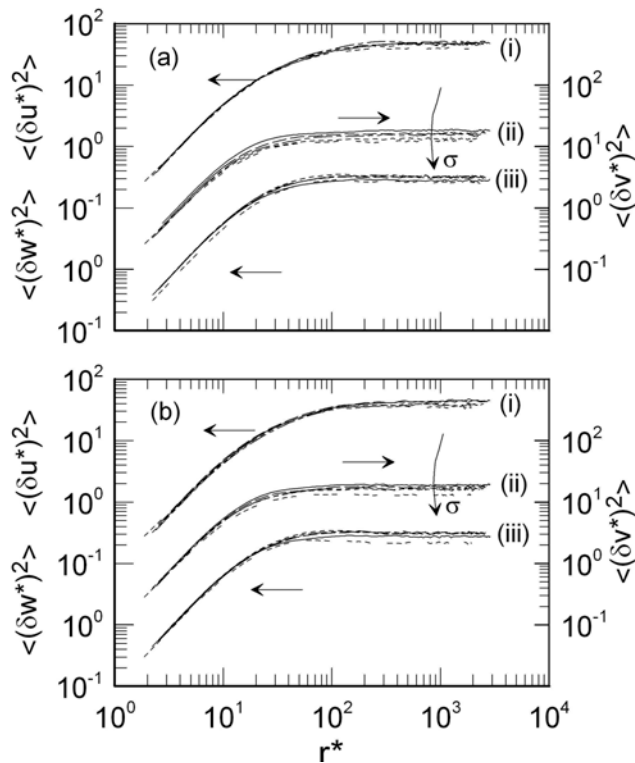


Figure 6: Kolmogorov normalized second-order velocity structure functions for several values of σ at (a) $y/\delta = 0.065$; (b) 0.125 . (i) $\langle(\delta u^*)^2\rangle$; (ii) $\langle(\delta v^*)^2\rangle$; (iii) $\langle(\delta w^*)^2\rangle$. Symbols are as in figure 5.

Conclusions

Some characteristics of the small-scale motion in a turbulent boundary layer subjected to concentrated suction, applied through a short porous wall strip, have been examined for a range of suction rates. The results indicate that, relative to no-suction, both R_λ and the normalised mean energy dissipation rate are reduced in the near-wall region when suction is applied,

suggesting that the structures in this region of the boundary layer have been modified. The Kolmogorov similarity hypothesis seem to be reasonably well satisfied for suction and no-suction data by spectra and second-order structure functions for $k^*_1 > 0.2$ and $r^* < 10$. However, Kolmogorov compensated spectra and second-order structure functions for $k^*_1 < 0.2$ and $r^* > 20$ depart from those for $\sigma = 0$, highlighting that suction induces a change in the small-scale motion as a result of the manipulation of the large-scale structures; the magnitude of this change increases as σ is increased.

Acknowledgments

The support of the Australian Research Council is acknowledged.

References

- [1] Antonia, R.A. and Kim, J., A Numerical Study of Local Isotropy of Turbulence, *Phys. Fluids*, **6**, 1994, 834-841.
- [2] Antonia, R.A., Kim, J. and Browne, L.W.B., Some Characteristics of Small-scale Turbulence in Turbulent Duct Flow, *J. Fluid Mech.*, **233**, 1991, 369-388.
- [3] Antonia, R.A., Zhu, Y. and Sokolov, M., Effect of Concentrated Wall Suction on a Turbulent Boundary Layer, *Phys. Fluids*, **7**, 1995, 2465-2475.
- [4] Durbin, P.A. and Speziale, C.G., Local Anisotropy in Strained Turbulence at High Reynolds Numbers, *Trans. ASME I: J. Fluids Engng.*, **113**, 1991, 707-709.
- [5] Kolmogorov, A.N., The Local Structure of Turbulence in Incompressible Viscous Fluid for Very Large Reynolds Number, *Dokl. Akad. Nauk. SSSR*, **30**, 1941, 301-305.
- [6] Lee, M.J., Kim, J. and Moin, P., Structure of Turbulence at High Shear Rate, *J. Fluid Mech.*, **216**, 1990, 561-583.
- [7] Martinez, D.O., Chen, S., Doolen, G.D., Kraichnan, R.H., Wang, L-P. and Zhou, Y., Energy Spectrum in the Dissipative Range of Fluid Turbulence, *J. Plasma Phys.*, **57**, 1997, 195-201.
- [8] Monin, A.S. and Yaglom, A.M., *Statistical Fluid Mechanics*. Vol. 2, 1975, MIT Press, Cambridge, MA.
- [9] Oyewola, O., Djenidi, L. and Antonia, R.A., Effect of Wall Suction on a Turbulent Boundary Layer: Reynolds Number Dependence, in *Proceedings of 14th Australasian Fluid Mech. Conf.*, editor B.B. Dally, Adelaide, 2001, 239-243.
- [10] Oyewola, O., Djenidi, L. and Antonia, R.A., Combined Influence of the Reynolds Number and Localised Wall Suction on a Turbulent Boundary Layer, *Expts. in Fluids*, **35**, 2003, 199-206.
- [11] Oyewola, O., Djenidi, L. and Antonia, R.A., Influence of Localised Wall Suction on the Anisotropy of the Reynolds Stress Tensor in a Turbulent Boundary Layer, *Expts. in Fluids*, **37**, 2004, 187-193.
- [12] Papailiou, D.D. and Lykoudis, P.S., Turbulent Vortex and the Entrainment Mechanism of the Turbulent Wake, *J. Fluid Mech.*, **62**, 1974, 11-31.
- [13] Sano, M. and Hirayama, N., Turbulent Boundary Layer with Injection and Suction Through a Slit. First Report: Mean and Turbulence Characteristics, *Bull. JSME*, **28**, 1985, 807-814.
- [14] Shah, D.A. and Antonia, R.A., Scaling of the Bursting Period in Turbulent Boundary Layer and Ducts Flows, *Phys. Fluids*, **A 1**, 1989, 318-325.
- [15] Spalart, P.R., Direct Simulation of a Turbulent Boundary Layer up to $R_\theta = 1410$, *J. Fluid Mech.*, **187**, 1988, 61-98.
- [16] Sreenivasan, K.R., On the Fine-scale Intermittency of Turbulence, *J. Fluids Mech.*, **151**, 1985, 81-103.
- [17] Sreenivasan, K.R., On the Universality of the Kolmogorov Constant, *Phys. Fluids*, **7**, 1995, 2778-2784.
- [18] Townsend, A.A. *The Structure of Turbulent Shear Flow*, 2nd ed., Cambridge, CUP, 1976.
- [19] Ueberoi, M.S., Equipartition of Energy and Local Isotropy in Turbulent Flows, *J. Appl. Phys.*, **28**, 1957, 1167-1170.